NOAA Technical Memorandum NMFS-AFSC-171

Vessel Comparison on the Seabed Echo: Influence of Vessel Attitude

by V. Hjellvik and A. De Robertis

U.S. DEPARTMENT OF COMMERCE
National Oceanic and Atmospheric Administration
National Marine Fisheries Service
Alaska Fisheries Science Center

May 2007

NOAA Technical Memorandum NMFS

The National Marine Fisheries Service's Alaska Fisheries Science Center uses the NOAA Technical Memorandum series to issue informal scientific and technical publications when complete formal review and editorial processing are not appropriate or feasible. Documents within this series reflect sound professional work and may be referenced in the formal scientific and technical literature.

The NMFS-AFSC Technical Memorandum series of the Alaska Fisheries Science Center continues the NMFS-F/NWC series established in 1970 by the Northwest Fisheries Center. The NMFS-NWFSC series is currently used by the Northwest Fisheries Science Center.

This document should be cited as follows:

> Hjellvik, V., and A. De Robertis. 2007. Vessel comparison on the seabed echo: Influence of vessel attitude. U.S. Dep. Commer., NOAA Tech. Memo. NMFS-AFSC-171, 34 p.

NOAA Technical Memorandum NMFS-AFSC-171

Vessel Comparison on the Seabed Echo: Influence of Vessel Attitude

by

Vidar Hjellvik[1] and Alex De Robertis[2]

[1] Institute of Marine Research,
P.O. Box 1870, Nordnes N-5817,
Bergen, Norway

[2]Alaska Fisheries Science Center
National Marine Fisheries Service
National Oceanic and Atmospheric Administration
7600 Sand Point Way NE,
Seattle WA 98115
www.afsc.noaa.gov

U.S. DEPARTMENT OF COMMERCE
Carlos M. Gutierrez, Secretary
National Oceanic and Atmospheric Administration
Vice Admiral Conrad C. Lautenbacher, Jr., U.S. Navy (ret.), Under Secretary and Administrator
National Marine Fisheries Service
William T. Hogarth, Assistant Administrator for Fisheries

May 2007

This document is available to the public through:

National Technical Information Service
U.S. Department of Commerce
5285 Port Royal Road
Springfield, VA 22161

www.ntis.gov

Notice to Users of this Document

This document is being made available in .PDF format for the convenience of users; however, the accuracy and correctness of the document can only be certified as was presented in the original hard copy format.

ABSTRACT

During an inter-vessel comparison of the NOAA ships *Oscar Dyson* and *Miller Freeman* in the Bering Sea in July 2006, significant vessel-differences in acoustic backscatter from walleye pollock (*Theragra chalcogramma*) were observed. However, very similar vessel-differences were observed in the seabed echo as well. Therefore, it was concluded that poorly understood differences in echosounder calibration or performance were likely the cause of the observed discrepancy in acoustic pollock backscatter from the two vessels. The seabed echo results were crucial to avoiding a faulty interpretation of differential vessel avoidance by fish in the water column. However, a careful examination of the seabed echo revealed that it was to some extent influenced by the pitch and the roll of the vessels. The most important pitch/roll variable during the inter-vessel comparison was the average roll (i.e., the list of the vessels). The seabed echo recorded by the NOAA ship *Miller Freeman* was more influenced by vessel list than was the seabed echo recorded by the NOAA ship *Oscar Dyson*. Since the sea was relatively calm during the experiment (wave height less than 2 m most of the time), the list effect was significant but small enough that the seabed echo could still be successfully used to help interpret echosounder output from both vessels. However, we believe that the effect could have been more severe under rougher sea conditions due to differential vessel motion, and – in fact – under very calm conditions as well, since the seabed echo may be extremely dependent on the incident angle of the acoustic beam, and a small deviance from zero incident angle could hence result in a too weak seabed echo. Therefore, the seabed echo must be interpreted with caution in all circumstances.

CONTENTS

INTRODUCTION

A new generation of noise-reduced research vessels is now being built around the world according to the recommendations for underwater-radiated noise levels developed by the International Council for the Exploration of the Seas (ICES) (Mitson 1995). The primary rationale for controlling low frequency underwater radiated noise is that there is a substantial body of evidence that fish can react to approaching research vessels (Olsen 1990, Mitson 1995, Misund 1997, Mitson and Knudsen 2003) and it is believed that it is the underwater noise emitted by these vessels that causes fish to avoid them. This is a major concern for stock assessment surveys using acoustic techniques since the method assumes that fish do not avoid the survey vessel. Thus, by making the new research vessels more silent, one would hope to reduce the problem of vessel-induced fish behavior.

One of these new vessels is the NOAA ship *Oscar Dyson*, which was built in 2003 for the U. S. National Oceanic and Atmospheric Administration (NOAA). The NOAA ship *Oscar Dyson* (OD) will soon be used as the primary vessel for acoustic surveys of stocks of walleye pollock *Theragra chalcogramma* in Alaska waters, which have traditionally been conducted with the NOAA ship *Miller Freeman* (MF). Although the *Miller Freeman* has been retrofitted with a new propeller designed to reduce radiated noise, the ship still produces low-frequency noise in the range of fish hearing which exceeds the ICES specifications for radiated noise (Gonzalez et al. 1999). If the *Oscar Dyson* actually causes less fish avoidance than the *Miller Freeman*, this may result in higher echo abundance measurements for the *Oscar Dyson*, even though the underlying fish abundance is not correspondingly higher. Thus, to ensure continuity in the fish abundance index time series used for fisheries management, it is important to inter-calibrate the two vessels. Because vessel avoidance behaviour is likely to be species and size-specific, and to depend on

other factors such as season and depth of the water column, the vessels should be compared under conditions representative of those encountered during surveys.

When undertaking such an inter-vessel comparison, it is crucial that the relationship between the output of the echosounder and the fish insonified by its transducer beam is the same for the two vessels. To ensure that this is the case, each echosounder is normally calibrated before or during the experiment using the standard sphere technique (Foote et al. 1987). Here, a standard target with known target strength is placed in the center of the acoustic beam to measure the sensitivity of the echosounder. Although this method provides precise measures of sensitivity, it does not measure the equivalent beam angle (EBA). The EBA is a parameter which accounts for the shape of the acoustic beam, which is important when estimating the density of objects such as fish that are distributed throughout the acoustic beam (i.e., not only in the center). In acoustic surveys, it is common practice to perform the on-axis calibration to establish echosounder sensitivity, but the equivalent beam angle is set to values provided by the manufacturer (Simmonds and MacLennan 2005). In part, this is because of the difficulty of measuring EBA. An alternative approach to echosounder calibration using a standard sphere is to compare echosounder output relative to the echo recorded from the seabed (Johannesson and Mitson 1983), and configure the echosounders such that they record the same echo strength from the bottom. Then, if the bottom echo is measured accurately, and the vessels pass over bottoms with similar characteristics, the echosounders will report similar echo intensity from the water column if they encounter similar fish aggregations. A comparison based on the strength of bottom echoes has the advantage that it will incorporate both the sensitivity of the echosounder and the shape of the beam. Although this method also has its pitfalls, it turned out to be crucial in the first vessel inter-comparison experiment between the *Miller Freeman* and the *Oscar Dyson*, which was performed in the Bering Sea in July 2006 (De Robertis et al., in review). In this report, we

provide a detailed description of the methodology we used to examine the impact of vessel motion on the bottom echoes recorded during this experiment.

MATERIALS AND METHODS

Study Design

An inter-vessel comparison of the *Miller Freeman* and the *Oscar Dyson* was conducted on 3-13 July 2006, concurrent with the biennial walleye pollock survey on the eastern Bering Sea shelf conducted by the *Miller Freeman* (Fig. 1a). The weather was calm with wind speed decreasing from around 22 knots on 3 July to around 10 knots on 13 July, and the wave height, as estimated by the bridge watch, was 2 m or less most of the time. The experimental design included a component in which the vessels travelled side-by-side at a separation of 0.5 nautical miles (nmi) along three 170-214 nmi transects during the acoustic survey (transects 22-24 in Fig. 1b). These transects were conducted using standard survey procedures (e.g. Honkalehto et al., 2002). An additional 215 nmi long transect was added as the vessels returned to port (transect 23.5 in Fig. 1b). For the side-by-side work, the *Oscar Dyson* was randomly displaced 0.5 nmi either to the east or west of the pre-planned *Miller Freeman* survey track line.

At 10 locations along the survey track lines, the side-by-side comparison was interrupted to conduct dedicated experiments (101-110, Fig. 1c-d) in which the vessels took turns "following the leader". The vessels conducted sets of 5.0 nmi east or west heading transects, with one vessel leading at a distance of ~1.0 nmi. Between 5 and 20 transects were conducted during each experiment, for a total of 101 transects. Preliminary analysis in the field after the first 36 transects were collected hinted toward lower echo abundance for the trailing vessel, potentially due to absorption from bubbles caused by the wake of the leading vessel. Due to this possible “lead

effect" (which eventually turned out to be very weak), the trailing vessel was displaced 0.1 nmi to the starboard side of the leading vessel for the subsequent 65 transects (experiments 105-110, Fig. 1d) in order to avoid the wake of the leading vessel. The lead vessel was assigned at random for each follow the leader transect. The bottom was very flat where the follow-the-leader experiments were conducted. The difference between maximum and minimum depth was less than 4 m for all of the 101 transects (on average 2.2 m).

Acoustic Data Collection

The NOAA ships *Miller Freeman* and *Oscar Dyson* are equipped with 18, 38, 120 and 200 kHz Simrad split-beam EK60 echosounders as well as the same model Simrad transducers. In order to minimize biases in echo integration measurements caused by shallow bubble layers the transducers were mounted on centerboards at depths of ~9.1 m (Ona and Traynor 1990). Echosounders were operated at power settings recommended by the manufacturer (Simrad 2002) to minimize range-dependent losses due to harmonic distortion (Tichy et al., 2003) at a ping interval of 1 per second. Pulse duration was set at 1 ms for all frequencies, and the same sound speed (1,470 m s^{-1}) and identical frequency-dependent absorption coefficients were used on both vessels. Other acoustic instruments were either turned off or synchronized to the EK60 echosounders in order to avoid acoustic interference.

The on-axis response of the echosounders was calibrated using the standard sphere technique (Foote et al. 1987) on several occasions during the survey. In the case of the *Miller Freeman*, calibrations were conducted on four occasions between 4 June and 25 July. For the *Oscar Dyson*, calibrations were conducted at the beginning and end of the intercomparison experiment, although two replicate measurements at 38 kHz were conducted on each occasion.

Processing of Acoustic Data

Acoustic data were post-processed using Sonardata Echoview software (3.50.54). The mean values (averaged in linear units) of integration gain from all available calibrations were applied to each frequency, and the manufacturer-supplied measurements of equivalent beam angle were used in post-processing. The echosign was primarily assigned to two categories, pollock and a near-surface class (mix) whose identity remains poorly known, but is thought to consist largely of jellyfish, macrozooplankton, and age 0 pollock. An additional bottom zone integrating the seabed echo was defined extending from the sounder detected bottom to 25 m below this point. Acoustic data from 15 m below the surface to 3 m off bottom were exported at a 1 m vertical and 0.1 nmi horizontal resolution.

Statistical Analysis of Echo Abundance

The analysis was conducted following the approach developed in Kieser et al. (1987). The measurements are modelled as

$$s_{A,i,j} = \alpha_j \rho_i \varepsilon_{i,j}, \quad i = 1,\ldots,n, \quad j = \text{OD, MF},$$

where $s_{A,i,j}$ is the s_A (nautical area scattering coefficient (m^2/nmi^2) recorded at transect part *i* by vessel j, ρ_i is the true fish density at transect part *i*, α_j is a vessel-specific scaling factor, and $\varepsilon_{i,j}$ is lognormally distributed random noise. We are interested in the vessel ratio

$$R = \alpha_{\text{OD}} / \alpha_{\text{MF}},$$

Defining

$$d_i = \ln(s_{A,i,OD}) - \ln(s_{A,i,MF}) = \ln(\alpha_{OD}) - \ln(\alpha_{MF}) + e_i ,$$

where $e_i = \ln(\varepsilon_{i,OD}) - \ln(\varepsilon_{i,MF})$ is normally distributed random noise, we have that $\hat{R} = \exp(\bar{d})$, where $\bar{d} = n^{-1}\sum_{i=1}^{n} d_i$, is an unbiased estimate of *R*. Assuming no autocorrelation in d_i, the 95% confidence interval for *R* is $\exp\left(\bar{d} \pm t_{n-1,0.025} s_d n^{-1/2}\right)$ where $t_{n-1,0.025}$ is the 2.5% quantile of the *t*-distribution with *n*-1 degrees of freedom.

With a 0.1 nmi horizontal resolution, d_i is highly autocorrelated, and we therefore aggregated the s_A in ESDUs (elementary sampling distance units) of 5 nmi. The ESDUs with mean s_A less than 20 for a given class (e.g., pollock, mix) for one or both of the vessels were excluded since at very low densities, d_i can easily become very large or very small if one vessel happens to observe fish that the other vessel doesn't detect. Also, a low s_A means we have less confidence that the echosign assignment is correct in the case of pollock.

Adjustment of Vessel Ratios to the Bottom Echo

As an alternate form of calibration, the vessel ratio *R* was scaled to the bottom echoes in order to control for poorly understood differences in calibration or echosounder performance that are manifested in the bottom echo. We calculated the vessel ratio $\hat{R}_{bot}$ for the seabed echo and used it to scale the observed vessel ratio $\hat{R}_{obs}$ for the backscatter from the water column as follows:

$$\hat{R}_{corr} = \hat{R}_{obs} - (\hat{R}_{bot} - 1) , \qquad (1)$$

To account for the biases introduced by physical separation of the vessels (during the side-by-side experiments they were 0.5 nmi apart) and vessel motion (see the next subsection), we only included transects from the follow-the-leader experiments in which the list of both ships was less than one degree. This procedure results in $\hat{R}_{corr} = 1$ for the bottom echoes from these transects (substitute $\hat{R}_{obs}$ in Equation 1 with $\hat{R}_{bot}$ to see this), and is analogous to calibrating the echosounders such that the same frequency instruments will report the same bottom backscatter strength.

Vessel Motion (Pitch and Roll) Data Collection

Pitch and roll data (angle in degrees) were collected on both vessels with a time resolution of ten observations per second with an Applanix POS MV 320 position and motion reference system. Pitch is defined as positive when the bow is higher than the stern, and the roll is positive when the starboard is higher than the port side. In addition, the inclination of the vessel relative to a flat position (i.e., the deviation from zero pitch and roll) was calculated as

$$\text{inclination} = \arctan\left(\sqrt{\tan^2(\text{roll}) + \tan^2(\text{pitch})}\right),$$

which is very close to $\sqrt{\text{pitch}^2 + \text{roll}^2}$ for pitch and roll < 10 degrees. Pitch, roll, and inclination were summarized by calculating the four statistics

$$\bar{x}_j = \frac{1}{n}\sum_{i=1}^{n} x_i, \quad \text{sd}(x)_j = \sqrt{\frac{1}{n-1}\sum_{i=1}^{n}\left(x_i - \bar{x}\right)^2}, \quad \overline{\text{abs}(x)}_j = \frac{1}{n}\sum_{i=1}^{n}|x_i|, \quad \max_i(|x_i|)_j \qquad (2)$$

for each one minute interval *j*, where *x* denotes either pitch, roll or inclination, and *n* is the number of recordings per minute (600). The mean and standard deviation (SD) statistics represent the point about which the motion occurs and the amplitude of the motion, respectively: for example, mean roll indicates if the boat is listed or not on average, whereas SD(roll) measures how much it rolls. These one minute summaries were again averaged over each 5 nmi transect of the follow-the-leader experiments as

$$\overline{y}_t = \sum_{j=1}^{N_t} y_j \ ,$$

where *t* denotes transect number, N_t is the duration in minutes of transect *t* (typically around 25 minutes) and *y* is one of the four statistics in Equation 2. These averages were calculated for each vessel separately, and the vessel difference (i.e., OD-MF) and vessel ratio (i.e., OD/MF) were also calculated. We use the notation

$$\overline{y}_{t,\mathrm{OD}}, \quad \overline{y}_{t,\mathrm{MF}}, \quad \overline{y}_{t,\mathrm{OD-MF}} = \overline{y}_{t,\mathrm{OD}} - \overline{y}_{t,\mathrm{MF}}, \quad \overline{y}_{t,\mathrm{OD/MF}} = \overline{y}_{t,\mathrm{OD}} / \overline{y}_{t,\mathrm{MF}}, \tag{3}$$

for the four cases, respectively.

Statistical Analysis of Seabed Echo and Vessel Motion

Linear and quadratic regressions of the seabed echo vessel ratio on pitch and roll data were performed as

$$r_t = b_0 + b_1 \overline{y}_t + \varepsilon_t \ \text{ and } \ r_t = b_0 + b_1 \overline{y}_t + b_2 \overline{y}_t^2 + \varepsilon_t \ , \tag{4}$$

where $r_t = s_{\mathrm{A,OD},t} / s_{\mathrm{A,MF},t}$ is the seabed echo vessel ratio, $\bar{y}_t$ is one of the four statistics in Equation 3, and ε_t is random noise.

A local variation index was calculated as

$$\Delta_{t,k}(x) = x_{t,k} - (x_{t-1,k} + x_{t+1,k})/2, \quad t_k = 2,\ldots,n_k - 1, \tag{5}$$

where x is the variable of interest, and n_k is the number of transects in experiment k, k = 1,…,10. To investigate how local changes in seabed echo vessel ratio were related to local changes in pitch and roll, we computed the regressions in Equation 4 with r_t (echo abundance ratio) and $\bar{y}_t$ (vessel motion) replaced by $\Delta_{t,k}(r)$ and $\Delta_{t,k}(\bar{y})$, respectively. Finally, we calculated a zigzag index, which indicates how the variable $\Delta_{t,k}(x)$ changes in experiment k as the vessel changes heading:

$$Z_k(x) = \frac{1}{n_k - 2} \sum_{t=2}^{n_k - 1} \Delta_{t,k}(x) \times I(\text{vessel is heading east}), \tag{6}$$

where $I(v)$ equals to 1 if v is true and to –1 if v is false. If $\Delta_{t,k}(x)$ tends to be positive when the vessel is heading east and negative when the vessel is heading west, we have $Z_k > 0$. In the opposite case, $Z_k < 0$, and with no specific pattern, $Z_k \approx 0$.

RESULTS

Echosounder Calibrations

On-axis calibrations were successfully accomplished for both ships with the exception of one case for the *Miller Freeman* 18 kHz where the appearance of large densities of fish in near-surface waters degraded the calibration results. This calibration was not included in further analyses. The on-axis calibrations exhibited relatively high precision over the study period: if we had chosen to apply any of the individual calibrations rather than the average of all calibrations, we would expect deviation of ~ 1-4% from the observed s_A, depending on the frequency (Fig. 2).

The 200 kHz echosounder aboard the *Miller Freeman* appeared to have a range-dependent bias with the echo intensity decreasing substantially with depth (Fig. 3). Therefore, it was excluded from the analysis in De Robertis et al. (in review). However, since there is little variation in the bottom depth for the data used in this work and as it is of interest to see how the effect of the vessel motion varies with frequency, we have chosen to include it here.

Vessel Ratio in Fish s_A and Seabed s_A

The estimated vessel ratio for pollock s_A varied substantially among the four frequencies, ranging from around 0.9 at 18 kHz to around 1.6 at 200 kHz (Fig. 4a), and it did not seem reasonable that a vessel difference in fish avoidance would be reflected so differently at the different frequencies. However, the same pattern was observed in the vessel ratio for the seabed s_A (Fig. 4b), meaning that the differences in backscatter recorded by the vessels are not caused by vessel avoidance by fish or other organisms. Rather, it must somehow be related to problems with the instrument calibration or echosounder performance. However, the on-axis calibrations performed during the study were quite precise (see above), and the observed vessel differences in s_A are too large to be accounted for solely by errors in the on-axis calibration. By normalizing

the echosounder output such that both vessels report the same mean seabed echo, we got much more consistent estimates among frequencies for the vessel ratio (Fig. 4c).

Effects of Pitch and Roll on Seabed s_A

Figure 5a shows the log-transformed seabed s_A for each vessel for each transect at 18 kHz, which was the frequency most affected by vessel motion. The vessel ratio $s_{A,OD} / s_{A,MF}$ is shown in Figure 5b. A clear zigzag pattern is seen in the vessel ratio, with a shift in direction between experiment 104 and 105. For the first four experiments the *Oscar Dyson* sees a relatively stronger seabed echo when the vessels are heading east, and for the last six when they are heading west. The apparent reason for this shift is that the wind changed from a head/tail wind to a side wind after experiment 104 (Fig. 6). The wind speed was about 20-25 knots during experiment 101 and decreased gradually to about 10-15 knots during experiment 110. The side wind induced zigzag pattern in the local variation index of seabed s_A is clearly strongest for the *Miller Freeman* (Fig. 5c-d, experiments 105-110), whereas the head/tail wind induced pattern is slightly stronger for the *Oscar Dyson* (Fig. 5c-d, experiments 101-104).

A corresponding zigzag pattern is evident in the pitch and roll data (Fig. 7). The amplitude (as indicated by the standard deviation) of both pitch and roll is largest for experiments 101-104, which is also the case for the east-west differences in pitch and roll amplitude (the distance between open and solid points). The averages of pitch and roll are more similar for experiments 101-104 and for 105-110, but there is a stronger east-west pattern for average roll (list) in the later experiments. In fact, the local variation in average roll (Equation 5), explains 77% of the local variation in seabed s_A for the *Miller Freeman*, whereas it only explains 1% for the *Oscar Dyson* (Fig. 8a). Thus, the list of the *Miller Freeman* appears to explain much more of the difference in seabed backscatter than does the list of the *Oscar Dyson*.

There also seems to be a connection between the roll for the *Miller Freeman* averaged over experiments (Fig. 7 top left) and the seabed s_A ratio averaged over experiments (Fig. 5b). In fact, 79% of the variation in the seabed s_A ratio averages at 18 kHz is explained by a linear regression on the *Miller Freeman* average roll (Fig. 8b). And if experiment 104 is left out, 96% is explained. Much of the high explanatory power comes from experiments 103 and 107 where the list of the *Miller Freeman* was largest (the two points in the upper left corner of Fig. 8b). For 38, 120 and 200 kHz, the corresponding r^2 values are 76%, 22% and 0% for all of the experiments and 88%, 48% and 10% with experiment 104 left out. Looking at individual transects rather than experiment averages, up to 71% of the variation in the seabed s_A ratio is explained by a linear regression on the *Miller Freeman's* average roll (Fig. 9a). In fact, the average roll for *Miller Freeman* explains far more of the variation in the seabed s_A ratio than any other single pitch/roll variable for any of the vessels, or the vessel ratio or vessel difference in any of the pitch/roll variables (Fig. 9a).

The pattern in the seabed echo for all frequencies is summarized for both ships in Figure 10. The zigzag patterns tend to be stronger for 38 kHz than for 18 kHz, particularly for the *Miller Freeman* for transects 101-104 and for the *Oscar Dyson* for transects 105-110. Still, the pitch and roll data explain less of the variation in the seabed s_A ratio for 38 kHz than for 18 kHz (Fig. 9b). Note also the similarities between the *Oscar Dyson* and the *Miller Freeman* (Fig. 10), especially for 18 kHz and transects 105-110 for 38 kHz. For 120 and 200 kHz the zigzag pattern is much weaker (Fig. 10), as is the explanatory power of the pitch and roll data (Fig. 9b). For 18 and 38 kHz there is a clear trend of getting a larger vessel ratio as the list increases, with the strength of the trend depending on which vessel is used to limit which data are included (Fig. 11). For 120 kHz the trend is in the same direction in Fig. 11a-c, but weaker, and for 200 kHz there is no clear trend. Excluding transects where |avg roll| > 1 for one or both vessels resulted in a reduction of bottom echo vessel ratio of about 0.04, 0.03, and 0.01 for 18, 38, and 120 kHz, respectively (Fig.

12). The pollock vessel ratio estimates $\hat{R}_{corr}$ (eq. 1) obtained by using the bottom adjustment based only on transects with |avg roll| < 1 degree for both vessels are shown in Figure 4d. Once the vessel ratios are corrected by the discrepancy in the bottom echoes, the frequency-dependence in the pollock vessel ratio largely disappears.

Finally, although there seems to be a relatively weak correlation between the lists of the two ships if we consider all experiments together, the within experiment correlation is quite strong (Fig. 13). This means that the vessels respond similarly to changes in heading, but that the mean list of the vessels varies with time. This is also reflected in the 18 kHz s_A through the parallelism of Z between the *Miller Freeman* and *Oscar Dyson* in Figure 10. Transects in the same direction (i.e., eastward or westward) within the same experiment tend to have more similar lists than transects from different experiments. This indicates that sea state is not the only factor that influences the seabed echo through the list. This suggests that changing vessel loads, for example moving of liquids between storage tanks from one experiment to next, may partly cause the list. This is likely the case as the vessels, particularly the *Miller Freeman*, are not designed to maintain even trim (M. Gallagher, commanding officer NOAA ship *Miller Freeman*, personal communication), and vessel trim will thus vary over time. Fuel is consumed from tanks in different locations aboard the vessel, and treated gray water is held in holding tanks and discharged periodically, which will impact the trim of the vessels during the experiment.

DISCUSSION

The intercomparison of echosounders based on the seabed echo was crucial to correctly interpreting the results from the inter-vessel comparison experiment with the *Oscar Dyson* and the *Miller Freeman* in the Bering Sea in July 2006 (cf. De Robertis et al. in review). Integration of the seabed echo has been informative in other applications as well (e.g., Dalen and Løvik 1981,

Johannesson and Mitson 1983). However, our work indicates that one should consider the effects of vessel attitude when interpreting the echo strength from the seafloor. An in-depth analysis of the data showed a clear relation between vessel motion and seabed echo for both vessels, especially at 18 and 38 kHz, but, as the sea was quite calm during our experiment, the impact of vessel motion on the seabed echo vessel ratio was relatively small in magnitude compared to the ratio in seabed echoes used to intercalibrate the echosounders. Still, we tried to eliminate the bias in the seabed calibration introduced by vessel list by only using transects with |avg roll| of less than one degree. This somewhat raised the estimates of the vessel ratio *R* in Figure 4d for 18, 38, and 120 kHz, and slightly lowered them for 200 kHz so that the 95% confidence intervals for the vessel ratios for pollock include one in all cases.

We suspect that the discrepancy between the seabed echoes for frequencies other than 200 kHz may be explained by biases in the equivalent beam angles (EBA) used to calibrate the echosounders. The on-axis calibration results were quite precise, and a likely explanation is that the on-axis standard sphere calibration method does not incorporate the equivalent beam angle, which is a measure of beam pattern. If the EBA supplied by the manufacturer is incorrect, this would result in a consistent offset between echosounders as observed in the echo integrations of pollock during the vessel intercomparison. By normalizing the echosounder to the seabed echo, we observed more consistent estimates among frequencies for the vessel ratio. This is primarily because seabed integrations incorporate the EBA as well as on-axis sensitivity, while the on-axis calibrations do not. Because of the difficulty of measuring EBA on installed transducers, this is rarely done during routine acoustic surveys (Simmonds and MacLennan 2005), although our measurements indicate that a better understanding of this quantity is needed for accurate acoustic surveys. Measurements of the EBA of a previous generation of transducers under highly controlled conditions (Simmonds, 1990) indicate that although EBA is stable over time, it can change depending on the mounting arrangement. Thus, even if the correct values of EBA are

supplied by the manufacturer, they may be incorrect and lead to biases once the transducers have been installed on a vessel.

In the case of the 200 kHz data, there appears to be a range-dependent loss in the case of the *Miller Freeman's* echosounder. It appears that the range correction for absorption and spreading of acoustic energy is inadequate, which suggests that the equipment is faulty. This increasing loss of signal with range is similar to what is expected in the case of harmonic distortion when transducers are driven at high power (Tichy et al. 2003). However, we suspect that this is not the case, as the echosounder power on both vessels was set to 100 watts, which is sufficiently low to avoid these problems (Simrad 2002). Additionally, if harmonic distortion was occurring, one would expect a similar effect on both echosounders. We thus suspect that equipment problems aboard the *Miller Freeman* are the cause, most likely a faulty transducer. The comparison of bottom echoes made it easy to diagnose the difference in echosounder performance on both vessels. It is important to note that there was no indication of the problem in the results of the sphere calibrations, which are typically conducted at a range of ~ 20 m and will not readily identify range-dependent biases.

If EBA is the cause of the frequency-dependent differences in echosounder output observed during the vessel intercomparison study discussed in this document, then the discrepancy between the EBA estimates on both ships at a given frequency should account for the observed ratio in the seabed echo. To decide if this actually is the case, reliable measurements of EBA are needed. A field technique to estimate the EBA on installed transducers has been developed (Reynisson 1998), but the precision of the technique is estimated to be ~ ±7%, which is insufficient to detect differences of ~10 % between two echosounders as we have observed in the case of the 18 and 38 kHz on the *Miller Freeman* and *Oscar Dsyon*. Resolving the issue of whether EBA is responsible for the observed discrepancies should have high priority, as the uncertainty in EBA will introduce biases in survey time series used for fisheries management

when vessels are changed or when transducers are replaced. If EBA is indeed the cause of our observations, and it can be quantified, this source of uncertainty can be accounted for and acoustic survey results will be more reliable.

Motivated by the EBA hypothesis, we disassembled the centerboards both vessels, and found that the EBA measurements specified by the manufacturer for the 18 kHz transducer on the *Miller Freeman* and the 38 kHz transducer on the *Oscar Dyson* were in fact for transducers with serial numbers that did not match the transducers physically installed on the vessels. Thus, the EBA used in the study for these two transducers were in fact incorrect. For the MF 18 kHz transducer this implied an overestimation of the backscatter by a factor of 1.096, and for the OD 38 kHz transducer the backscatter was underestimated by a factor of 0.977. After correcting for this discrepancy, the vessel ratio at 18 kHz was close to 1.0, whereas for 38 kHz it was still around 1.1 (cf. Fig. 5 in De Robertis et al. in review). Thus, for the case of 18 kHz, the bottom comparison did identify a discrepancy in EBA as suspected, illustrating the utility of bottom echo comparison. Development of new methods for precise and accurate characterization of equivalent beam angle is thus still a priority.

The pollock s_A did not exhibit the same zigzag pattern as did the seabed s_A, which is reasonable since the acoustic signal behaves differently when encountering fish and the seabed. Although backscatter from fish (including pollock) is directional (e.g., Hazen and Horne 2003), the seabed echo is much more directional. The intensity of acoustic backscatter from the seabed is extremely dependent on the incident angle, particularly for sediment covered seabeds like those in the eastern Bering Sea (Talukdar et al. 1995). For example, at an incident angle of ~ 2 degrees which is equivalent to the maximum average vessel list observed in his study, the seabed echo is several decibels less than that when the incident angle is zero (Talukdar et al. 1995). In comparison the reflectivity of swimbladdered fish such as pollock is much less sensitive to such small differences in incident angle (e.g., Foote 1985, Hazen and Horne, 2003).

In summary, the measurement of the ratio in seabed echoes was helpful in this application, but it is important to recognize that intercalibration on the seabed is not without error. Although it may appear surprising at first, calm conditions and a flat seabed are not necessarily the best conditions for intercalibration on the seafloor echo. In the case of a very flat seabed, and calm conditions, specular reflections from the seabed may be important, and the seabed echo may be very dependent on the incident angle of the acoustic beam (Urick 1983, Talukdar et al. 1995). The mean incident angle will be affected by vessel trim and the pointing angles of the transducers, which will alter the echo from the seafloor. Our observations of an alternating pattern in the seabed echo associated with changes in heading are consistent with this mechanism: As the vessel changes heading, pitch and roll change, and there is a corresponding change in the bottom echo. Our results indicate that a change of only one or two degrees in vessel trim have detectable effects on the bottom ratio. Thus, vessel motion, particularly list, can impact the bottom echo strength and must be considered when intercalibrating on the seafloor echo. Including all transects would have resulted in bottom echo ratios that were up to 0.04 higher than those computed from transects where the list was less than one degree (Fig. 12). This difference is relatively small, but it will likely be much larger in more severe winds and seas due to accentuated differential vessel motion in higher sea sates, and on vessels with different trim. There is remaining uncertainty in the bottom adjustment even after limiting the analysis to low list cases, and the confidence intervals for the vessel ratios corrected for the bottom echoes are thus slightly too narrow, although it is difficult to quantify by exactly how much. In this application, however, the bottom echo analysis has been informative, as it has allowed us to attribute the frequency-dependent discrepancies in pollock backscatter to echosounder performance or calibration rather than differential vessel avoidance by fish.

ACKNOWLEDGEMENTS

This work is the product of the efforts of a great many people, without whom the study would not have been possible. Members of the Alaska Fisheries Science Center (AFSC) acoustics group, particularly J. Millstein, C. Wilson, N. Williamson, S. Furnish, R. Towler, P. Ressler, D. McKelvey, K. Williams and D. Twohig contributed to various aspects of this work. The comments of P. Ressler, M. Jech, and N. Williamson improved the manuscript. We would like to thank the command and crew of NOAA ships *Miller Freeman* and *Oscar Dyson* for their assistance and careful ship handling. We would also like to express our appreciation to those who prepared the vessels for this work, including members of the NOAA Marine Operations Center, Pacific, and members of NOAA Fisheries' Office of Science and Technology, particularly M. Bancroft. This work was supported by AFSC. V. Hjellvik's participation was made possible by the Norwegian Research Council through the Strategic Institute Program for IMR ("Absolute abundance estimation of fish" 143249/140).

CITATIONS

Dalen, J., and A. Løvik. 1981. The influence of wind-induced bubbles on echo integration surveys. J. Acoust. Soc. Am. 69:1653-1659.

De Robertis, A., V. Hjellvik, N. Williamson, and C. Wilson. in review. Silent ships do not always encounter more fish: comparison of acoustic backscatter recorded by a noise-reduced and a conventional research vessel. Submitted to ICES J. Mar. Sci.

Foote, K. G. 1985. Rather high-frequency sound scattering by swimbladdered fish. J. Acoust. Soc. Am. 78:688-700.

Foote, K. G., H. P. Knudsen, G. Vestnes, D. N. MacLennan, and E. J. Simmonds. 1987. Calibration of acoustic instruments for fish density estimation: a practical guide. Coop. Res. Rep. Cons. int. Explor. Mer. 144. 69 p.

Gonzalez, A., B. Kollars, B. Harris, B., and B. Kipple. 1999. *Miller Freeman* (R/V 233) Post conversion / diagnostic acoustic trial results. Naval Surface Warfare Center Carderock Division - 71 - TR 1999/187 164 p.

Hazen, E. L., and J. K. Horne. 2004. Comparing the modeled and measured target-strength variability of walleye pollock, *Theragra chalcogramma*. ICES J. Mar. Sci. 61:363-377.

Honkalehto, T., N. J. Williamson, S. de Blois, and W. Patton. 2002. Echo integration-trawl survey results for walleye pollock (*Theragra chalcogramma*) on the Bering Sea Shelf and Slope during summer 1999 and 2000. U.S. Dep. Commer. NOAA Tech. Memo. NMFS-AFSC-125-126 66p.

Johannesson, K. A., and R. B. Mitson. 1983. Fisheries acoustics. A practical manual for aquatic biomass estimation. FAO Fish. Tech. Paper 240. 249 p.

Kieser, R., T. J. Mulligan, N. J. Williamson, and M. O. Nelson. 1987. Intercalibration of two echo integration systems based on acoustic backscattering measurements. Can. J. Fish. Aquat. Sci. 44:562-572.

Misund, O. A. 1997. Underwater acoustics in marine fisheries and fisheries research. Rev. Fish Biol. Fish. 7:1-34.

Mitson, R. B. Editor. 1995. Underwater noise of research vessels: review and recommendations. ICES Coop. Res. Rep. 209. 61 p.

Mitson, R. B., and H. P. Knudsen. 2003. Causes and effects of underwater noise on fish abundance estimation. Aquat. Liv. Res. 16:255-263.

Olsen, K. 1990. Fish behaviour and acoustic sampling. Raupp. P-v. Reun. Cons. int. Explor. Mer 189: 147-158.

Ona, E., and J. J. Traynor. 1990. Hull mounted, protruding transducer for improving echo integration in bad weather. ICES CM 1990/B31.

Reynisson, P. 1998. Monitoring of equivalent beam angles of hull-mounted acoustic survey transducers in the period 1983-1995. ICES J. Mar. Sci. 55:1125-1132.

Simrad. 2002. Non-linear effects: Recommendation for fishery research investigations. Simrad News Bulletin, March 2002

Simmonds, E. J. 1990. Very accurate calibration of a vertical echo sounder: a five-year assessment of performance and accuracy. Raupp. P-v. Reun. Cons. int. Explor. Mer 189: 183-191.

Simmonds, E. J., and D. N. MacLennan. 2005. Fisheries Acoustics 2nd. Ed. Blackwell Science. Oxford, UK, 437 p.

Talukdar, K. K., R. C. Tyce, and C. S. Clay. 1995. Interpretation of sea beam backscatter data collected at the Laurentian Fan off Nova Scotia using acoustic backscatter theory. J. Acoust. Soc. Am. 97:1545-58.

Tichy, F. E., H. Solli, and H. Kaveness. 2003. Non-linear effects in a 200-kHz sound beam and the consequences for target strength measurement. ICES J. Mar. Sci. 60:571-574.

Urick, R. J. 1983. Principles of underwater sound. 3rd Edition. McGraw-Hill, New York. 424 p.

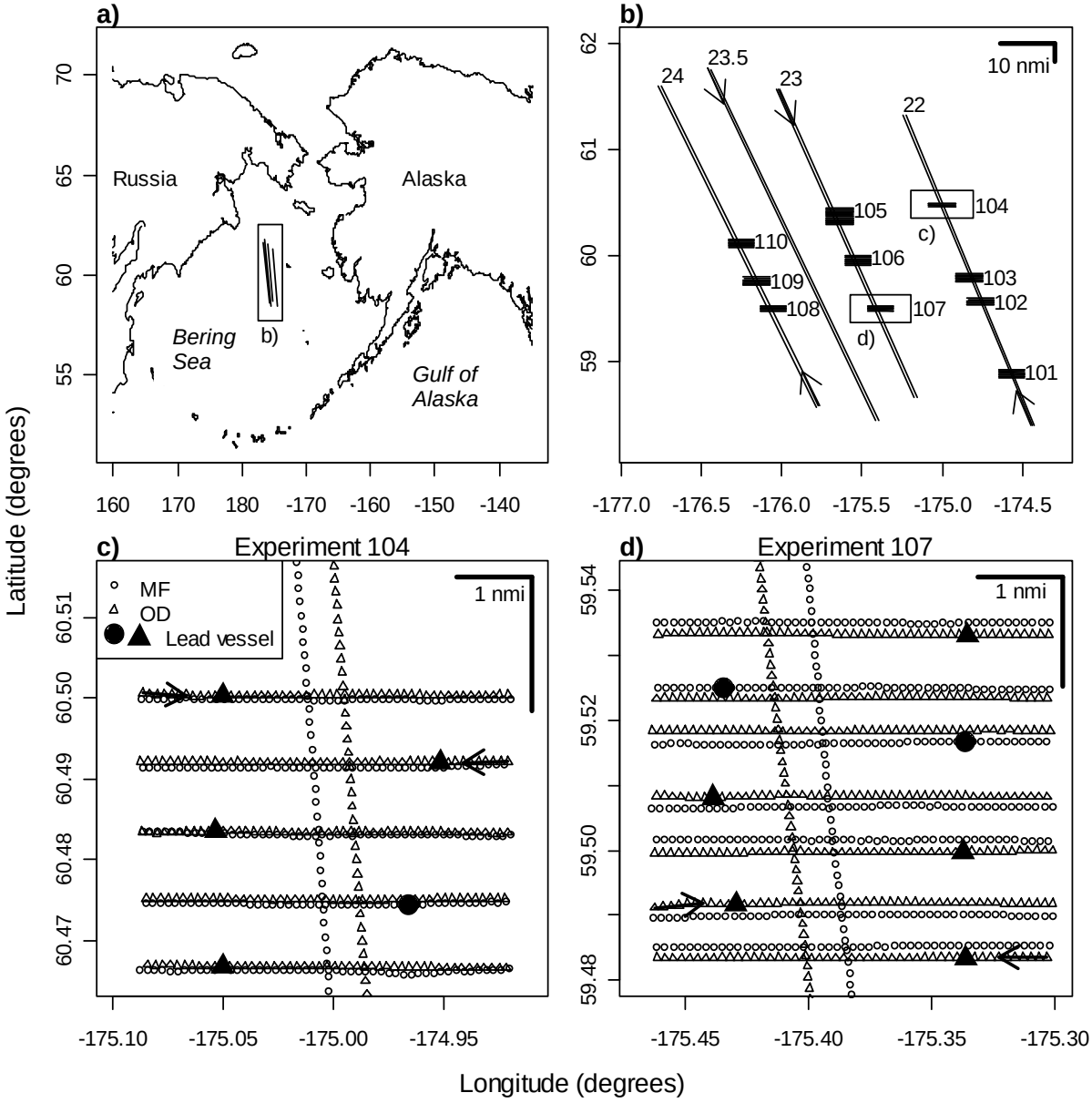

Figure 1. -- Experimental design. a) Location of the experiment. b) Standard transects (22-24,23.5) and dedicated transects (101-110). Arrows indicate direction of travel. c) Details of transect 104 and a part of transect 22. Each point is the start of a 0.1 nmi segment. Arrows indicate cruising direction for the two first transect parts (changes for each transect part). The large symbols indicate the position of the lead vessel (*Miller Freeman* (MF) if triangle, *Oscar Dyson* (OD) if circle) when the trailing vessel starts on each transect part. d) Same as c) for transect 107.

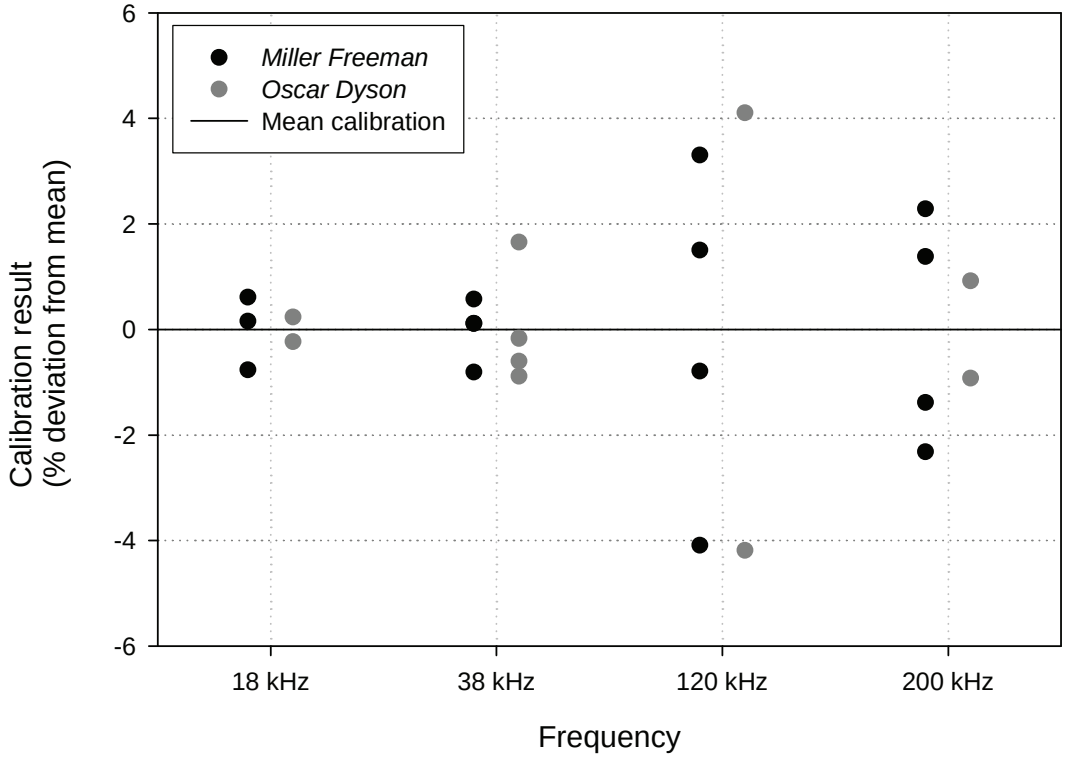

Figure 2. -- Impact of using a single on-axis sphere calibration on s_A measurements reported in this study compared to applying the mean integration gain from all calibrations combined. Each plotted point indicates the impact of using only this calibration on echo-integration measurements compared to applying the average integration gain from all calibration as has been applied in this study. Results are expressed as Percent Deviation $= \left(2 \cdot \left(Gain - \overline{Gain}\right) / \overline{Gain}\right) \cdot 100$, where *Gain* corresponds to the on-axis integration gain in linear units. The calculation accounts for the two-way effects of integration gain on echo integration. Although four calibrations were conducted at 38 kHz for *Miller Freeman*, in two of the cases, results were very similar and thus, only three distinct points are visible on the graph.

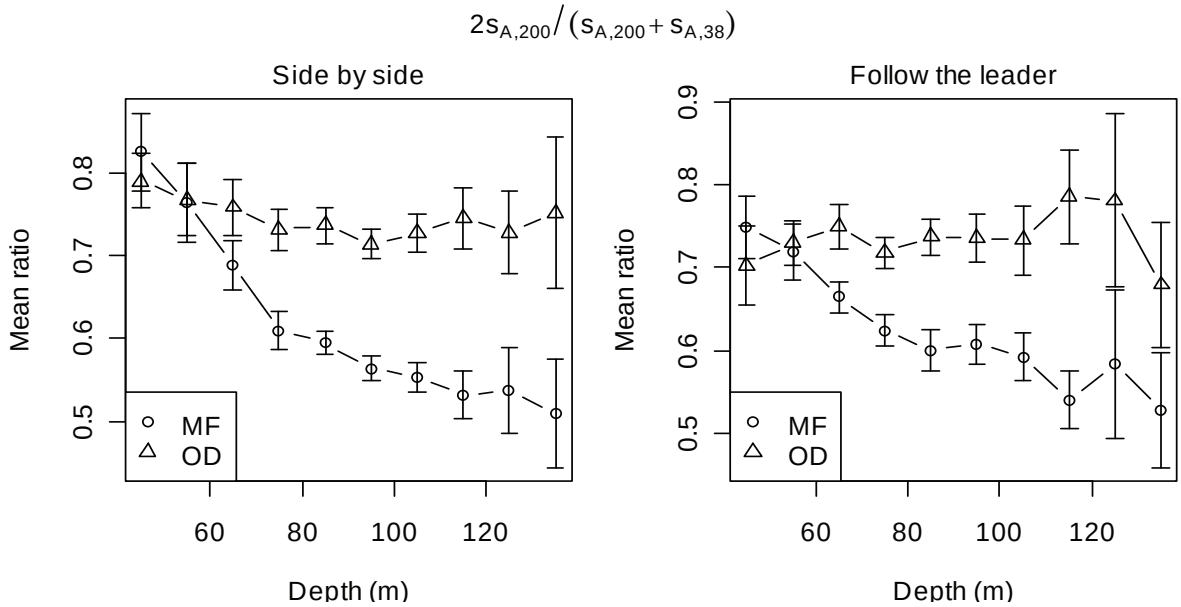

Figure 3. -- 200 kHz echosounder performance as a function of depth and vessel. The ratio $s_{A,200}/\{(s_{A,200}+s_{A,38})/2\}$ for pollock as a function of depth and vessel is shown. For each elementary sampling distance unit the ratio was calculated for all 10 m depth layers with $s_A > 1$. The figure shows the mean ratio ± 2 standard errors for each depth layer.

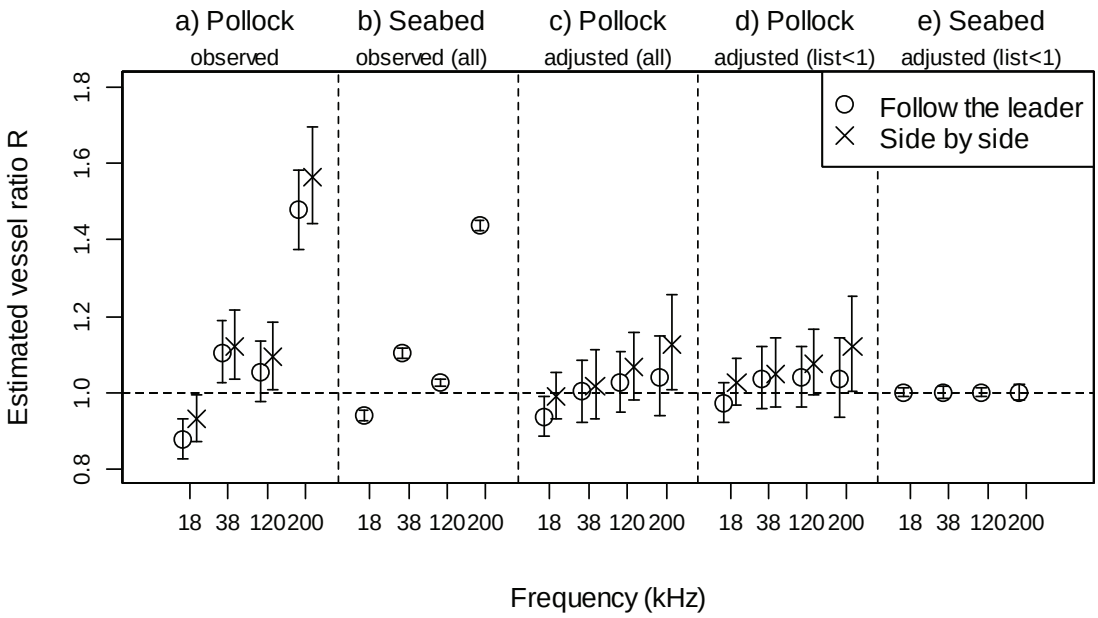

Figure 4. -- Estimated vessel ratios (α_{OD} / α_{MF}) with 95% confidence intervals. a,c,d): Vessel ratios for pollock based on a) sphere calibrations, c) seabed adjustments using all transects, and d) seabed adjustments using transects where |list| < 1 for the *Oscar Dyson* and the *Miller Freeman*. b): Vessel ratios for the seabed, using all transects, based on sphere calibrations. e): Vessel ratios for the seabed, using seabed transects where |list| < 1 for both vessels, based on seabed adjustments using the same transects.

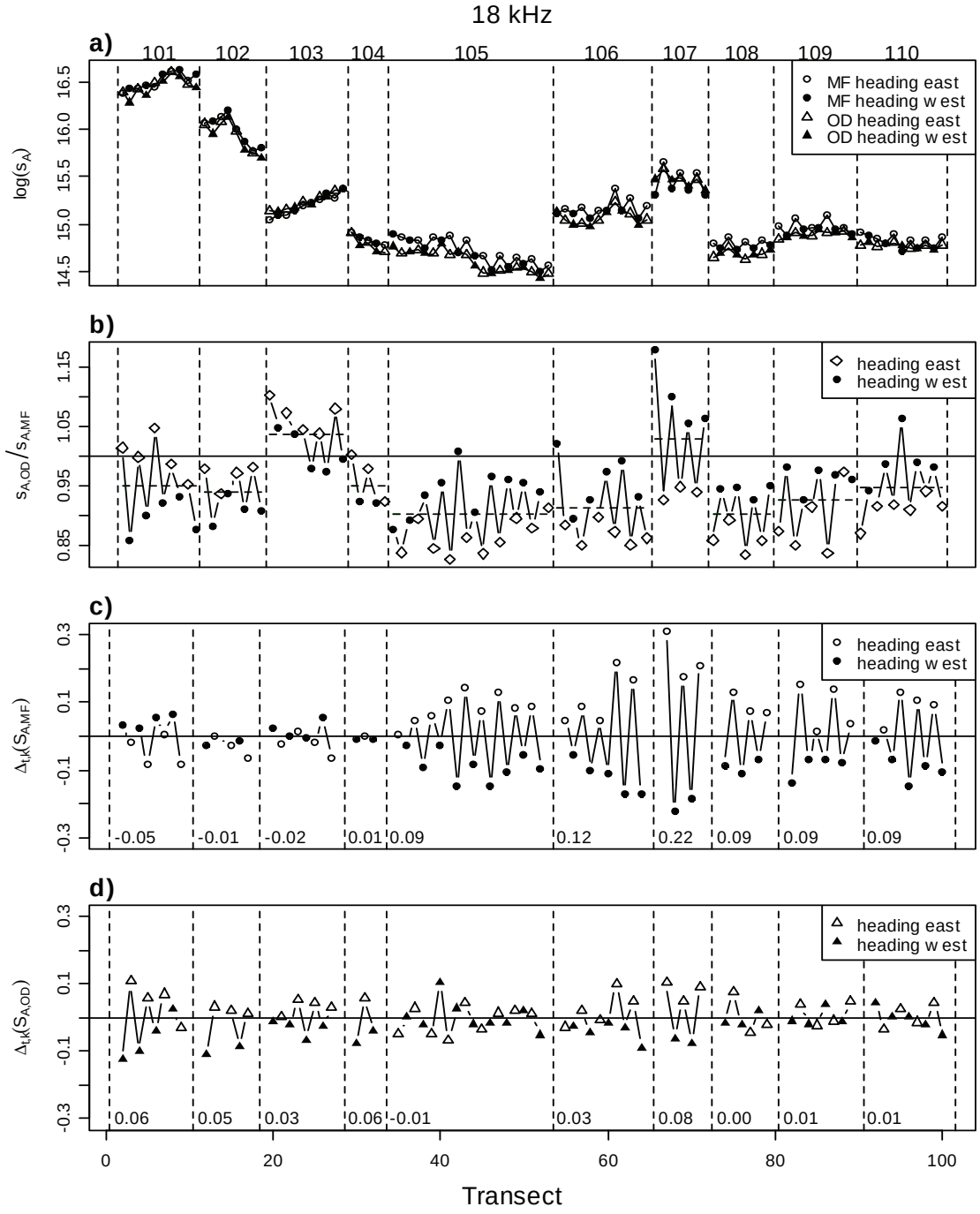

Figure 5. -- Seabed echo at 18 kHz. a) Log-transformed seabed echo for *Miller Freeman* (MF) and *Oscar Dyson* (OD). Dashed vertical lines demarcate individual experiments. b) Vessel ratios. Dashed horizontal lines indicate mean vessel ratio within each experiment. c) The local variation index $\overline{y}_t^{\Delta}$ defined in Equation 5 for MF. Transect 4 of experiment 102 is omitted since this peak seems to be due to changes in seabed properties. The numbers at the bottom show the zigzag index defined in eq. 6. d) Same as c) but for OD.

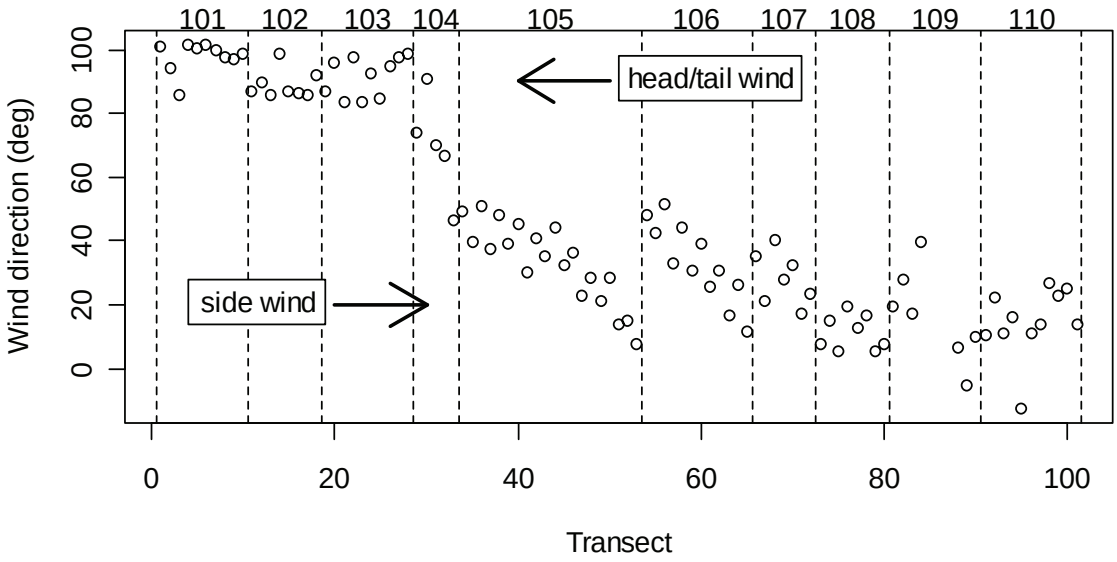

Figure 6. -- Average wind direction observed during each of the follow-the-leader transects. Experiments are indicated above the figure and are separated by the vertical dotted lines.

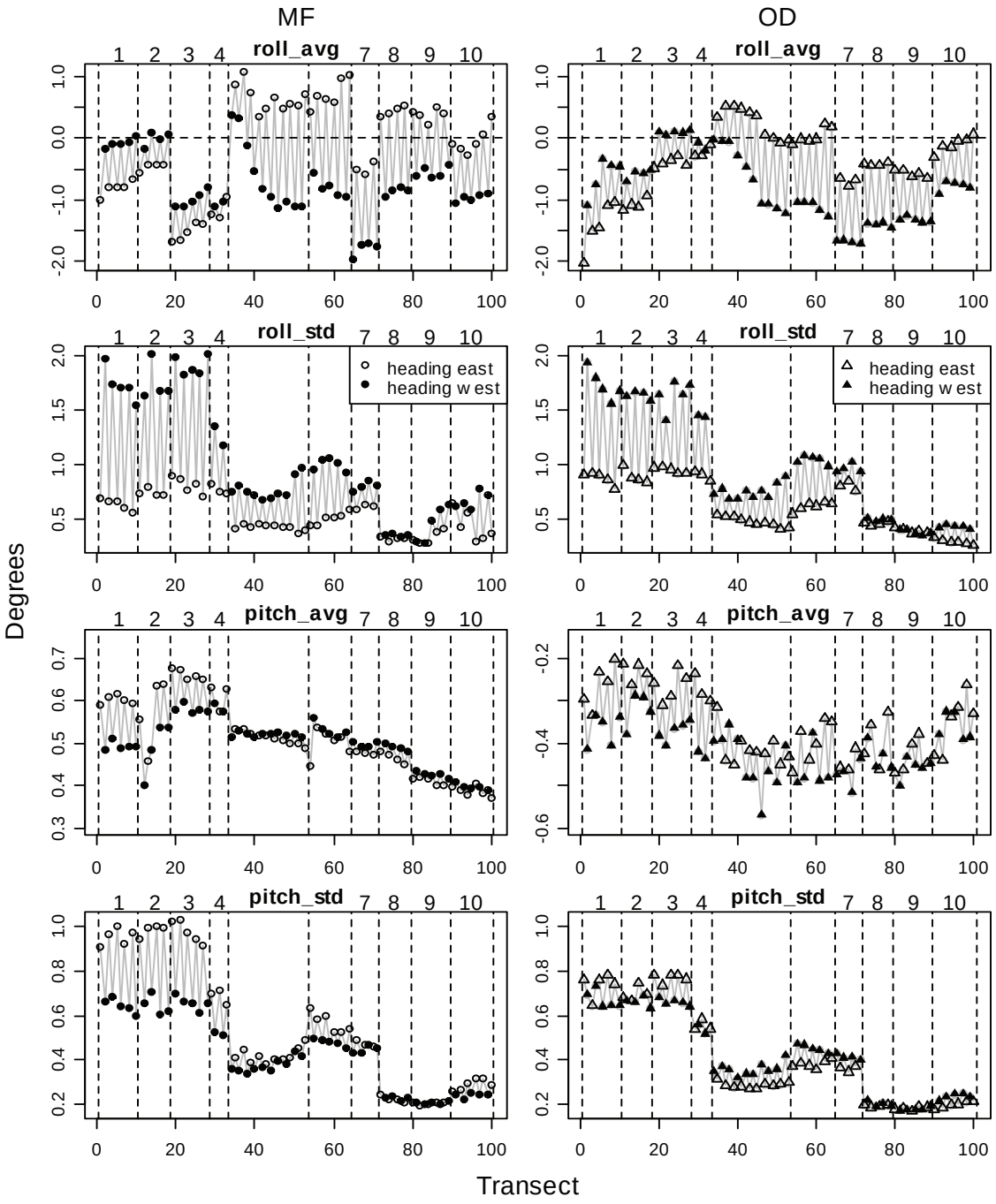

Figure 7. -- Average and standard deviation of pitch and roll measurements recorded during each follow-the-leader transect.

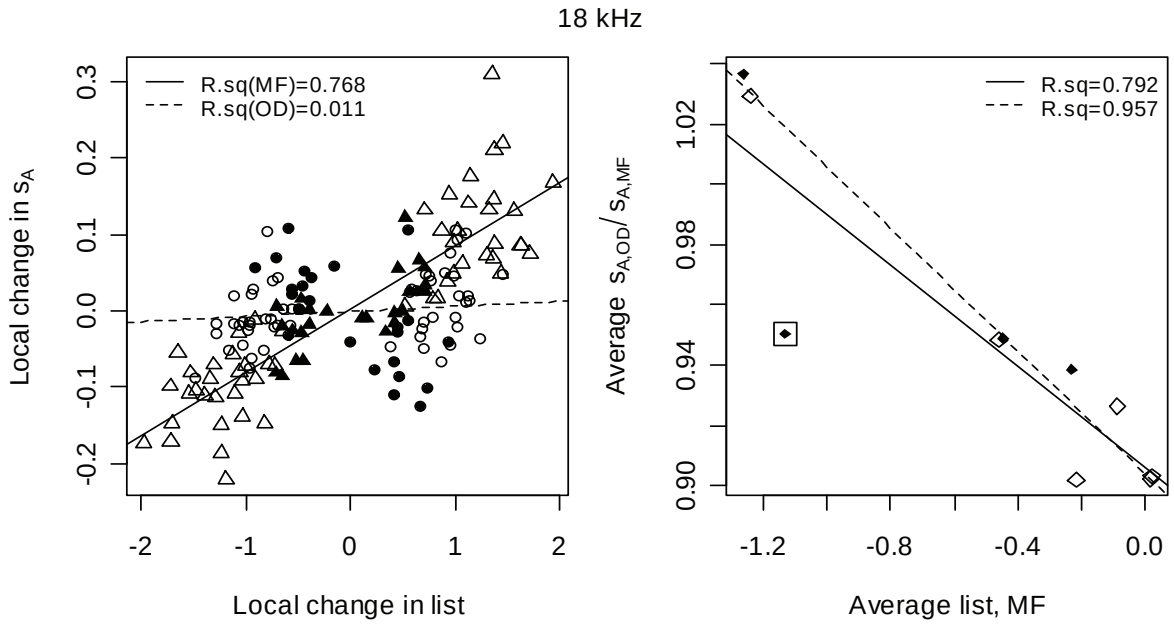

Figure 8. -- Left: Local change in seabed s_A ($\Delta_{t,k}(\bar{y})$, cf. eq. 5) at 18 kHz plotted against local change in average roll ($\Delta_{t,k}(r)$) for *Miller Freeman* (circles) and *Oscar Dyson* (triangles) with linear regression lines and R-squared values. Filled symbols are used for experiments 101-104. Right: Average seabed s_A ratio for each experiment plotted against average list for MF. Triangles are used for experiments 101-104. Experiment 104 is boxed. The solid regression line and r^2 value includes experiment 104, while the black line and corresponding r^2 value does not.

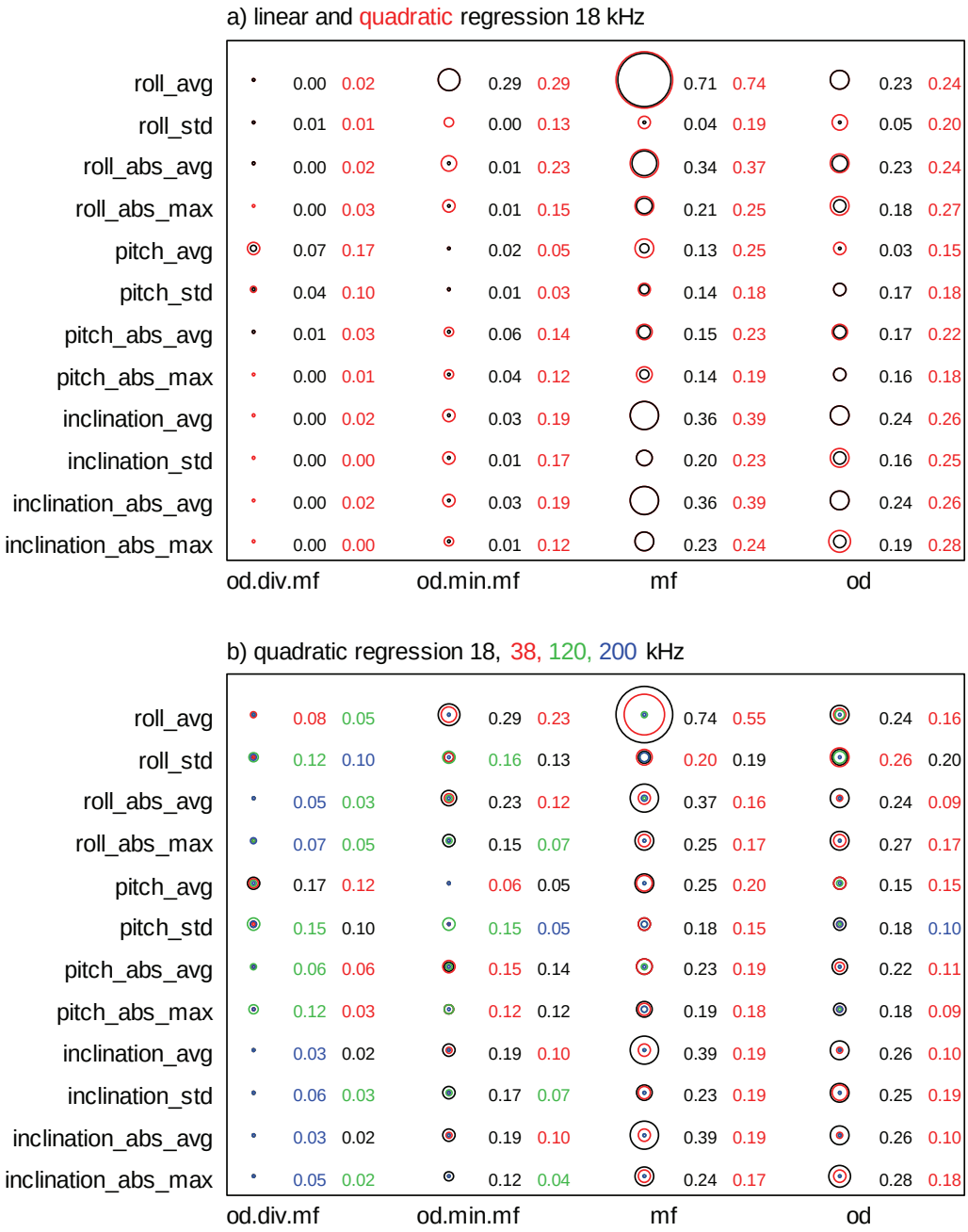

Figure 9. -- a) The variation in seabed s_A ratio explained by linear (black) and quadratic (red) regression of various explanatory variables. The diameter of the circles is proportional to r^2, which is given to the right of the circles. In the first column the *Oscar Dyson* (OD) values are divided by the *Miller Freeman* (MF) values for the explanatory variables, in the second column the values for MF are subtracted from the values of OD, in the third and fourth column, the values from MF and OD only, are used. b) The same for quadratic regression for 18 (black), 38 (red), 120 (green) and 200 (blue) kHz. The two highest r^2 values are given in each case, with the color corresponding to the frequency.

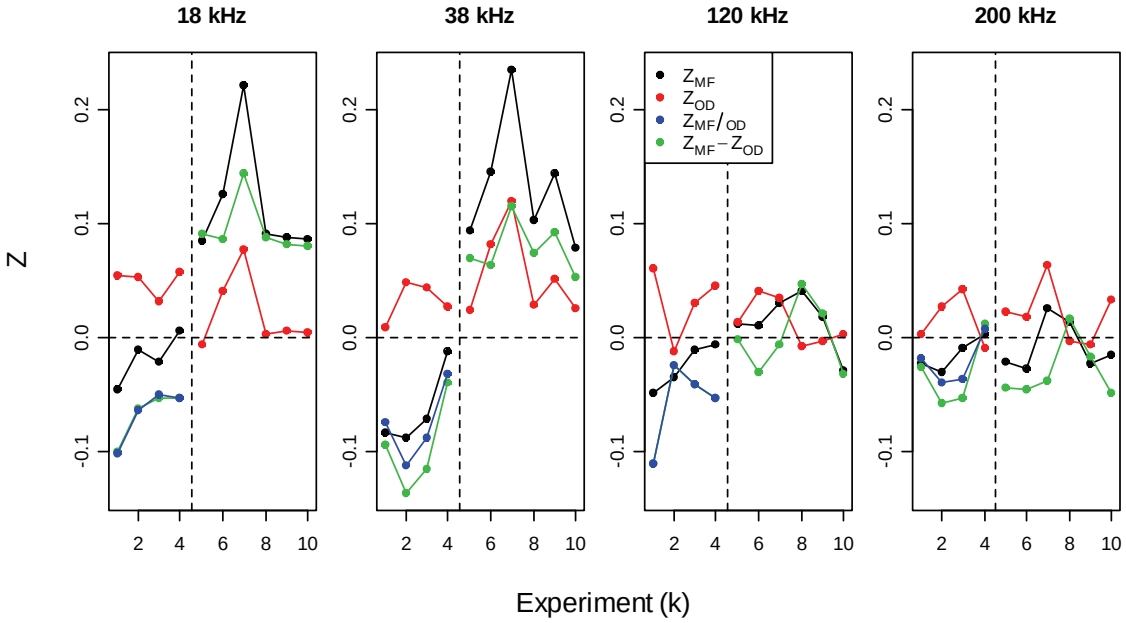

Figure 10. -- The zigzag indices (Equation 6) Z_k (ln($s_{A,MF}$)) (black), Z_k (ln($s_{A,OD}$)) (red), and Z_k ($s_{A,MF}$/ $s_{A,OD}$) (blue) as a function of experiment and frequency. The green points show Z_k (ln($s_{A,MF}$)) - Z_k (ln($s_{A,OD}$)).

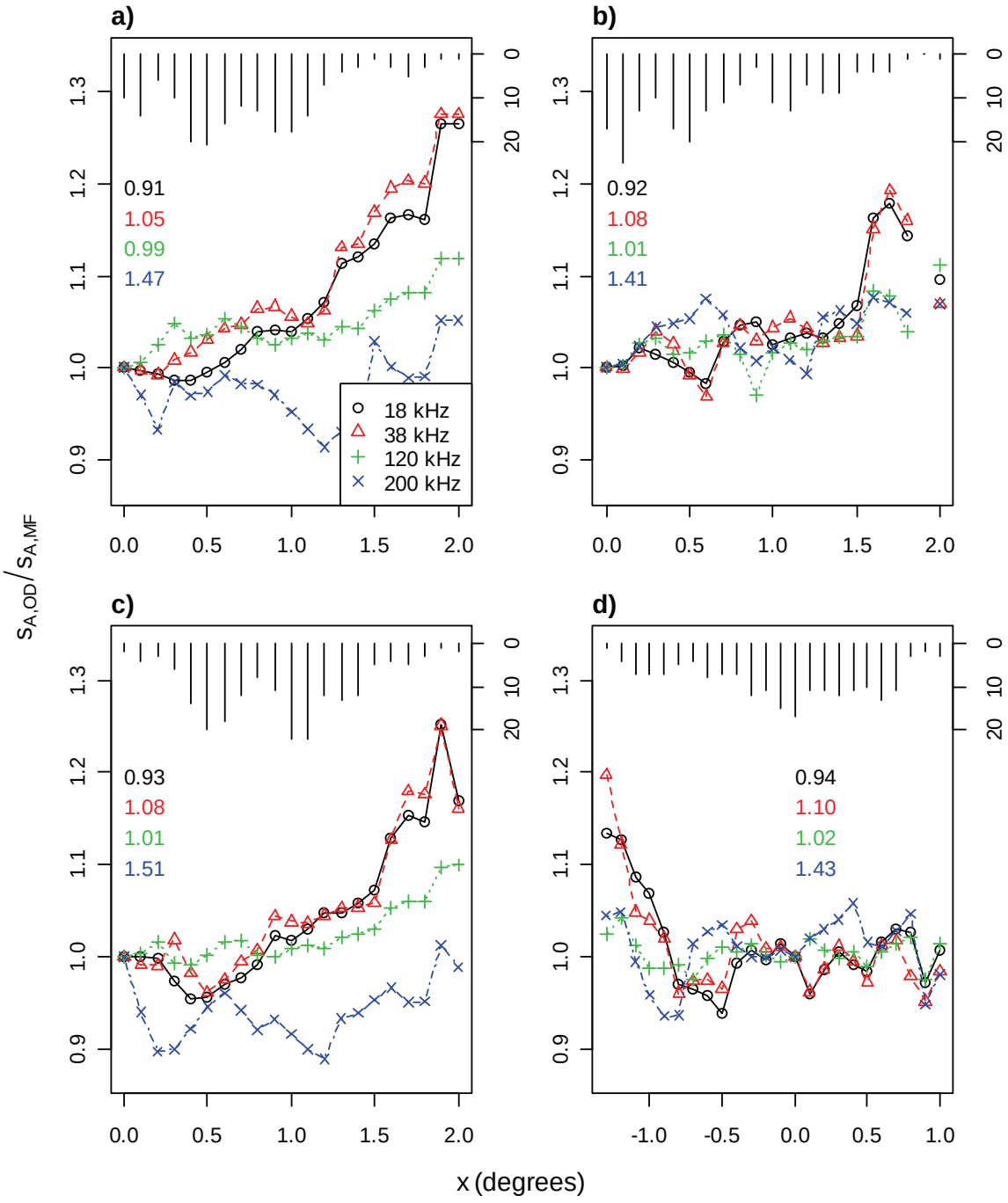

Figure 11. -- The vessel ratio as a function of average roll $\bar{R}$. Each point is based on segments where $|\bar{R}_{MF}|$ (a), $|\bar{R}_{OD}|$ (b), max($|\bar{R}_{MF}|$,$|\bar{R}_{OD}|$) (c), or $|\bar{R}_{OD}| - |\bar{R}_{MF}|$ (d) is within [x – 0.1 , x + 0.1], where x is the value on the x-axis. All curves are adjusted vertically so that $y = 1$ when $x = 0$ for the adjusted curves. The actual vessel ratios at $x = 0$ are given by the numbers in the plots. The number of segments that each point is based on is indicated in the histograms at the top of each plot.

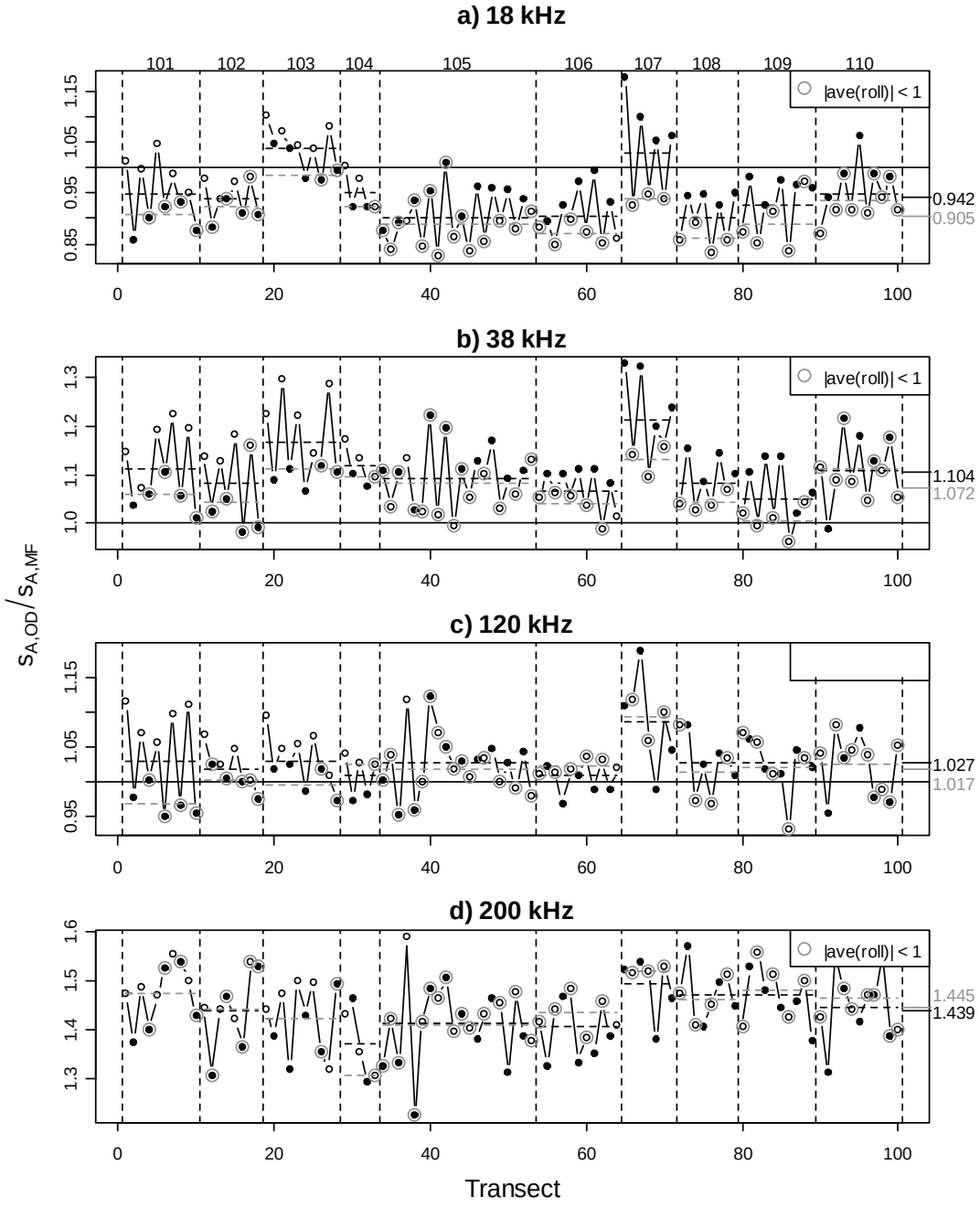

Figure 12. -- Vessel ratio in seabed s_A for 18, 38, 120 and 200 kHz. Gray circles indicate cases where the condition |avg(roll)}<1| is fulfilled for both vessels. The gray numbers in the right margin are the average vessel ratios calculated from these transects only. The black numbers are the average vessel ratios calculated from all transects. The gray and black dashed lines are the experiment means of the gray and black points, respectively.

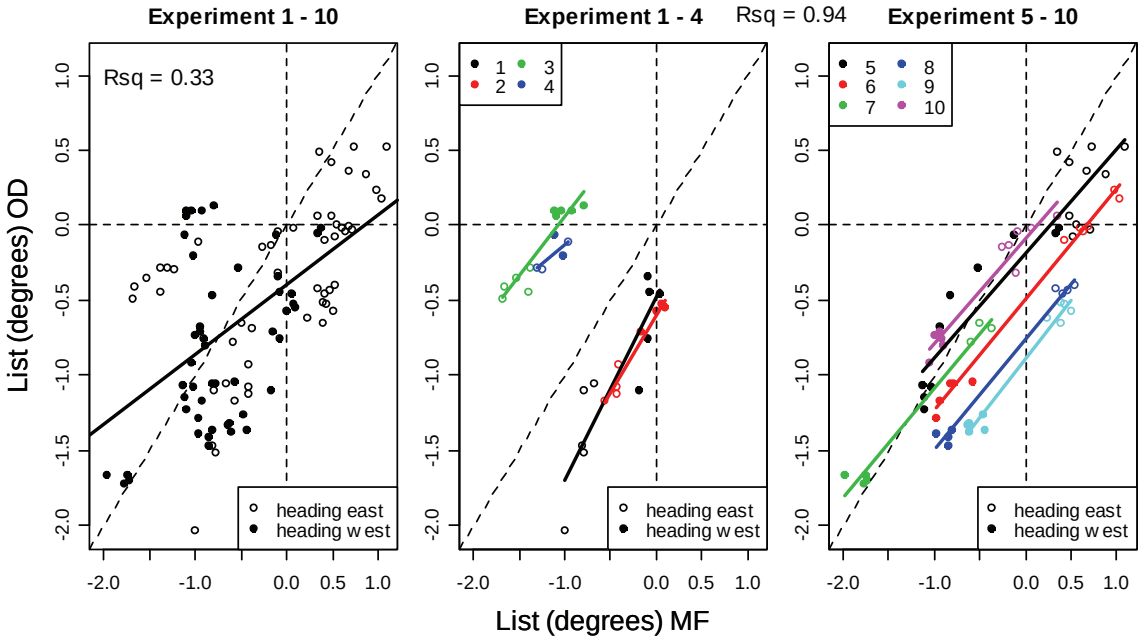

Figure 13. -- The list for the *Miller Freeman* (MF) plotted against the list for the *Oscar Dyson* (OD) (one point per transect), with regression lines for all experiments joined together (left) and each for experiment by itself (middle and right). The dashed lines indicate list(MF) = list(OD).

RECENT TECHNICAL MEMORANDUMS

Copies of this and other NOAA Technical Memorandums are available from the National Technical Information Service, 5285 Port Royal Road, Springfield, VA 22167 (web site: *www.ntis.gov)*. Paper and microfiche copies vary in price.

AFSC-

170 RODGVELLER, C. J., J. H. MOSS, and A. M. FELDMANN. 2007. The influence of sampling location, timing, and hatching origin on the prediction of energy density in juvenile pink salmon, 27 p. NTIS number pending.

169 PELLA, J., and J. MASELKO. 2007. Probability sampling and estimation of the oil remaining in 2001 from the *Exxon Valdez* oil spill in Prince William Sound, 58 p. NTIS number pending.

168 ANGLISS, R. P., and R. B. OUTLAW. 2007. Alaska marine mammal stock assessments, 2006, 244 p. NTIS No. PB 2007-106476.

167 PEREZ, M. A. 2006. Analysis of marine mammal bycatch data from the trawl, longline, and pot groundfish fisheries of Alaska,1998-2004, defined by geographic area, gear type, and catch target groundfish species, 194 p. NTIS No. PB2007-106475.

166 WING, B. L, M. M. MASUDA, and S. G. TAYLOR. 2006. Time series analyses of physical environmental data records from Auke Bay, Alaska, 75 p. NTIS No. PB2007-101890.

165 EILER, J. H., T. R. SPENCER, J. J. PELLA, and M. M. MASUDA. 2006. Stock composition, run timing, and movement patterns of Chinook salmon returning to the Yukon River Basin in 2004, 107 p. NTIS No. PB2007-102224.

164 YANG, M-S., K. DODD, R. HIBPSHMAN, and A. WHITEHOUSE. 2006. Food habits of groundfishes in the Gulf of Alaska in 1999 and 2001, 199 p. NTIS number pending.

163 EILER, J. H., T. R. SPENCER, J. J. PELLA, and M. M. MASUDA. 2006. Stock composition, run timing, and movement patterns of chinook salmon returning to the Yukon River basin in 2003, 104 p.NTIS No. PB2006-108429.

162 IGNELL, S. E., B. L. WING, B. D. EBBERTS, and M. M. MASUDA. 2006. Abundance and spatial pattern of salps within the North Pacific Subarctic Frontal Zone, August 1991, 26 p. NTIS No. PB2006-108423.

161 ANGLISS, R. P., and R. OUTLAW. 2005. Alaska marine mammal stock assessments, 2005, 247 p. NTIS number pending.

160 SEPEZ, J. A., B. D. TILT, C. L. PACKAGE, H. M. LAZARUS, and I. VACCARO. 2005. Community profiles for North Pacific fisheries - Alaska, 552 p. NTIS No. PB2006-108282.

159 ETNIER, M. A., and C. W. FOWLER. 2005. Comparison of size selectivity between marine mammals and commercial fisheries with recommendations for restructuring management policies, 274 p. NTIS No. PB2006-102327.

158 LANG, G. M., P. A. LIVINGSTON, and K. A. DODD, 2005. Groundfish food habits and predation on commercially important prey species in the eastern Bering Sea from 1997 through 2001, 222 p. NTIS number pending.

157 JOHNSON, S. W., A. DARCIE NEFF, and J. F. THEDINGA. 2005. An atlas on the distribution and habitat of common fishes in shallow nearshore waters of southeastern Alaska, 89 p. NTIS number pending.

156 HOFF, G. R., and L. L. BRITT. 2005. Results of the 2004 Eastern Bering Sea upper continental slope survey of groundfish and invertebrate resources, 276 p. NTIS No. PB2006-100504.